A Generic Tri-Band Matching Network

Mohammad A. Maktoomi, *Graduate Student Member, IEEE*,
Mohammad S. Hashmi, *Member, IEEE*, Ajay P. Yadav, and Vishal Kumar

***Abstract*—A scheme to achieve impedance matching at three arbitrary frequencies is presented. The proposed matching network is cascade of a dual-band matching network and a novel dual-to-tri-band transformer. Analysis of the proposed network provides closed form design equations that enable physically realizable solution owing to the presence of a free design variable. The presented theory is demonstrated through two example prototypes on Roger's RO4350B substrate. The obtained simulated and measured results clearly exhibit the potential of the proposed design.**

***Index Terms*—Coupler, dual-band, impedance transformer, matching network, power amplifier, power divider, tri-band.**

I. Introduction

Matching networks are integral part of many RF/microwave devices such as amplifiers, mixers, oscillators, antennas and power dividers/combiners. Furthermore, multi-band/multi-standard devices require matching networks operating at more than one frequency.

Dual-band impedance matching techniques have been widely reported [1]–[4], but tri-band impedance matching approach is still in infancy [5]–[9]. The tri-band impedance transformer [5] is only an approximate result based on curve fitting whereas the one reported in [6] is limited due to the use of lumped components. Other tri-band matching networks [7], [8] are based on coupled lines and require compensation for different even-odd mode velocities when implemented in microstrip technology while the multiband impedance inverter network [9] is unable to work at arbitrarily chosen desired frequencies.

In this letter, for the first time, a systematic design of a tri-band matching network using only distributed components is presented. The proposed technique overcomes limitations of earlier techniques [5]–[9], and is extremely simple, versatile, and easily realizable.

II. Proposed Tri-Band Matching Network

Illustration of the proposed tri-band impedance transformer is shown in Fig. 1. Its aim is to match the load impedance R_L (shown at the extreme right) to the source impedance, Z_0 ($= 50\ \Omega$, shown at the extreme left) at three arbitrary frequencies, say, f_1, f_2, and f_3 such that, $f_1 < f_2 < f_3$. It is apparent that the design utilizes a dual-band impedance transformer (*DBIT*). Although, any *DBIT* from the existing literature could be selected, the two examples in this letter make use of the

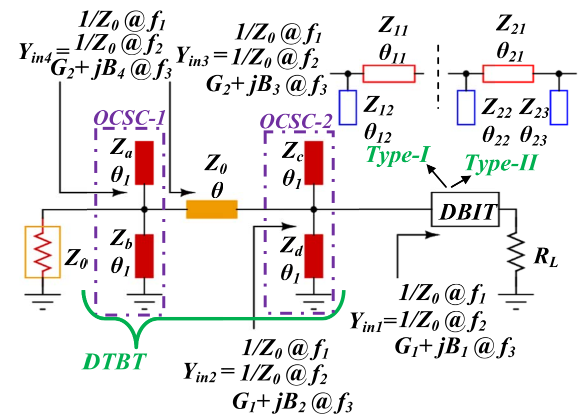

Fig. 1. Proposed tri-band matching network.

DBIT concepts of type-I [1] and type-II [2]. In series with the *DBIT*, there is a *dual to tri-band transformer* (*DTBT*). In Fig. 1, OCSC-1, OCSC-2, and a transmission-line (*TL*) segment of electrical length θ and characteristic impedance Z_0 (i.e., same as the source impedance) are the three constituents of the proposed *DTBT*. The constituents OCSC-i $\{i \in 1, 2\}$ are parallel combination of open and short stubs with electrical lengths θ_1 and respective characteristic impedances Z_a (Z_c) and Z_b (Z_d). All the electrical lengths are defined at the first frequency, f_1, and $\forall\, i : Y_i = 1/Z_i$. It is important to recall that the electrical length is proportional to frequency for non-dispersive lines [3], so the electrical length θ defined at f_1 is equal to $u\theta$ at f_3, for example, with $u = f_3/f_1$.

The working of the proposed tri-band transformer, given in Fig. 1, is as follows. Matching at the first two frequencies f_1 and f_2 is established by *DBIT*. The *DTBT* is designed in such a way that it doesn't alter the matching at these two frequencies. The role of *DTBT* comes into picture only at third frequency, f_3 and therefore, $Y_{\rm in1} = Y_{\rm in2} = Y_{\rm in3} = Y_{\rm in4} = 1/Z_0$ @ f_1 & @ f_2 is always valid. In general, the value of $Y_{\rm in1}$ @ f_3 will be of the form $G_1 + jB_1$, where G_1 and B_1 depends on whether the *DBIT* is of type-I or type-II, besides the value of R_L. The expressions of G_1 and B_1 are given at the end, after references.

The *DTBT* is ineffective @ f_1 and f_2 as the TL-segment does not alter the matching established by *DBIT* @ f_1 and f_2 considering the characteristic impedance of the same was chosen as equal to source impedance (i.e., Z_0), and the OCSC-i $\{i \in 1, 2\}$ have an infinite input impedance at f_1 and f_2.

Y_p, the admittance of OCSC-1 is given by

$$Yp = \frac{1}{jZ_b \tan\theta_1} - \frac{1}{jZ_a \cot\theta_1}. \tag{1}$$

Infinite impedance of OCSC-1 requires that Y_p be set to zero. And, therefore, the following expression is obtained from (1):

$$Z_a = Z_b \tan^2\theta_1. \tag{2}$$

Manuscript received July 31, 2015; revised December 26, 2015; accepted January 18, 2016. Date of publication April 29, 2016; date of current version May 6, 2016.

The authors are with IIIT Delhi, New Delhi, 110020, India (e-mail: ayatullahm@iiid.ac.in; mshashmi@iiitd.ac.in; ajaypratap12125@iiitd.ac.in; vishal12170@iiitd.ac.in).

Color versions of one or more of the figures in this letter are available online at http://ieeexplore.ieee.org.

Digital Object Identifier 10.1109/LMWC.2016.2548981

Moreover, for the condition in (2) to be simultaneously satisfied @ f_1 and f_2, a condition for θ_1 is given by [3]

$$\theta_1 = \frac{(1+s)\pi}{1+r} \tag{3}$$

where s is an integer and $r = f_2/f_1$.

Similarly, for OCSC-2 to present an infinite impedance, Z_a and Z_b can be replaced by Z_c and Z_d, respectively, in (2) and that result into

$$Z_c = Z_d \tan^2 \theta_1. \tag{4}$$

Furthermore, admittance Y_{in3} @ f_3 can be expressed as

$$Y_{\text{in3}}|_{f_3} = \frac{1}{Z_0} \frac{Z_0 + jZ_{\text{in2}}|_{f_3} \tan u\theta}{Z_{\text{in2}}|_{f_3} + jZ_0 \tan u\theta} = G_2 + jB_3 \tag{5}$$

where

$$G_2 = \frac{G_1(1+\tan^2 u\theta)}{(1 - Z_0 B_2 \tan u\theta)^2 + (Z_0 G_1 \tan u\theta)^2} \tag{6}$$

$$B_3 = \frac{(1 - Z_0 B_2 \tan u\theta)(Z_0 B_2 + \tan u\theta) - Z_0^2 G_1^2 \tan u\theta}{Z_0 \left[(1 - Z_0 B_2 \tan u\theta)^2 + (Z_0 G_1 \tan u\theta)^2\right]} \tag{7}$$

where, $u = f_3/f_1$, and

$$\begin{aligned} B_2 &= B_1 + Y_c \tan \mathrm{u}\theta_1 - Y_d \cot \mathrm{u}\theta_1 && \text{(8a)} \\ &= B_1 + Y_c(\tan \mathrm{u}\theta_1 - \tan^2 \theta_1 \cot \mathrm{u}\theta_1). && \text{(8b)} \end{aligned}$$

Similarly, admittance Y_{in4} @ f_3 can be expressed as follows:

$$Y_{\text{in4}}|_{f_3} = G_2 + jB_4 \tag{9}$$

where

$$\begin{aligned} B_4 &= B_3 + Y_a \tan \mathrm{u}\theta_1 - Y_b \cot \mathrm{u}\theta_1 && \text{(10a)} \\ &= B_3 + Y_a(\tan \mathrm{u}\theta_1 - \tan^2 \theta_1 \cot \mathrm{u}\theta_1) && \text{(10b)} \end{aligned}$$

and, therefore, the matching is achieved at f_3, if the following constraints are imposed:

$$G_2 = \frac{1}{Z_0} \tag{11}$$

$$B_4 = 0 \tag{12}$$

(6) and (11) are solved simultaneously to arrive at

$$\tan u\theta = \frac{Z_0 B_2 \pm \sqrt{(Z_0 B_2)^2 - (1 - Z_0 G_1)\left(Z_0^2 B_2^2 + Z_0^2 G_1^2 - Z_0 G_1\right)}}{\left(Z_0^2 B_2^2 + Z_0^2 G_1^2 - Z_0 G_1\right)}. \tag{13}$$

Once the value of θ is known from (13), the equations (2), (7), (8a-b), (10a-b), and (12) can be simplified to find the admittance, Y_a, as

$$Y_a = -\frac{B_3}{\tan u\theta_1 - \tan^2 \theta_1 \cot u\theta_1}. \tag{14}$$

It is obvious from (7) and (8a-b) that B_3 depends on B_2 which in turn depends on Z_c. This is one extremely important parameter of the proposed tri-band matching network. The term Z_c can be considered a free variable that can be selected appropriately to get a physically realizable transformer. In practice, for realizable microstrip, the value of Z_c lies between 30 to 150 Ω.

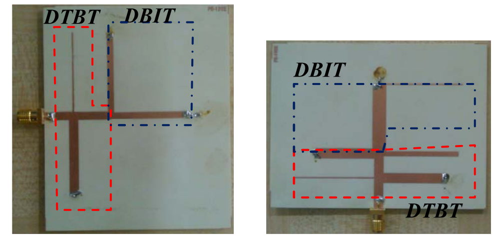

(a) (b)

Fig. 2. Fabricated devices (a) example-I (b) example-II.

III. Design Procedure

The design steps are summarized as follows:

1) **Step-I**: For a given R_L, calculate the parameters $Z_{11}, \theta_{11}, Z_{12}, \theta_{12}$ for type-I *DBIT* or $Z_{21}, \theta_{21}, Z_{22}, \theta_{22}, Z_{23}, \theta_{23}$ for type-II *DBIT* using the equations given in [1] or [2]. This design should be validated through simulation.
2) **Step-II**: Calculate $Y_{\text{in1}}|f_3 = G_1 + jB_1$ using the formula (A1a) and (A1b) or (A2a) and (A2b) depending upon the type of *DBIT* or preferably by simulation.
3) **Step-III**: In some cases, OCSC-2 may not be required (thus, $B_2 = B_1$). Hence, all the tri-band design should start with this assumption. Value of Z_a is evaluated using (13) and (14). Out of the two values from (13), only that value of θ is used which gives physically realizable transformer. Impedance Z_b is calculated from (2).
4) **Step-IV**: If values of *TL*s of *DTBT* are not within the realizable 30 Ω to 150 Ω range, then the design procedure is repeated by considering use of OCSC-2 assuming a value for Z_c. It will be useful to write a MATLAB code incorporating various design equations and then sweep the value of Z_c from 30 Ω to 150 Ω. Choose only that value of Z_c which gives physically realizable transformer parameters. It may be noted that the side stub of *DBIT* may be combined with stubs of OCSC-2, as done here in the example-II of the next section.

IV. Design Examples

As a case study, two design examples, while assuming f_1, f_2, and f_3 as 1 GHz, 2 GHz, and 2.5 GHz respectively, are given to demonstrate the effectiveness of the proposed matching network. The first example makes use of type-I *DBIT* whereas the second uses a type-II *DBIT*. Both the designs are prototyped on RO4350B substrate of thickness 1.524 mm and a copper cladding of 35 μm.

A. Design Example-I With Type-I DBIT

In this example, $R_L = 100\ \Omega$ is taken. Using the design procedure, the values of various lines for the *DBIT* are found to be $Z_{11} = 57.735\ \Omega$, $\theta_{11} = 60°$, and $Z_{12} = 57.735\ \Omega$, $\theta_{12} = 60°$. The admittance Y_{in3} @ $f_3 = 0.012 + j0.024\ \Omega^{-1}$is found through simulation. Using the design equations, the design values of *DTBT* are found to be $Z_a = 141.42\ \Omega$, $Z_b = 47.14\ \Omega$, $\theta_1 = 60°$, and $\theta = 60.166°$. OCSC-2 is not required in this case as the design values are physically realizable. The fabricated board is shown in Fig. 2(a) and the corresponding EM simulated and the measured results are shown in Fig. 3(a). The agreements of simulated and measured results at the three bands demonstrate the effectiveness of the proposed design.

$$B_1 = \frac{2Z_{21}B_P + \tan u\theta_{21} - Z_{21}^2 R_L^2 \tan u\theta_{21} - 3Z_{21}^2 B_P^2 \tan u\theta_{21} - B_P Z_{21} \tan^2 u\theta_{21} + B_P^3 Z_{21}^3 \tan^2 u\theta_{21} + R_L^2 B_P Z_{21}^3 \tan^2 u\theta_{21}}{Z_{21}\left((1 - B_P Z_{21} \tan u\theta_{21})^2 + (R_L Z_{21} \tan u\theta_{21})^2\right)} \tag{A2b}$$

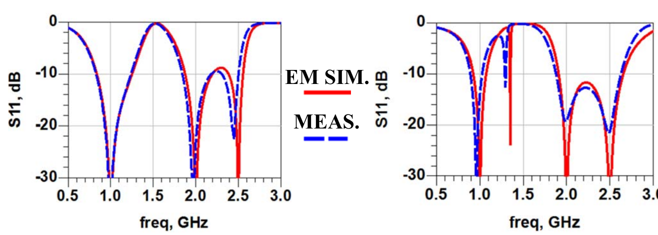

(a) (b)

Fig. 3. Simulation and measurement results (a) example-I (b) example-II.

TABLE I
COMPARISON WITH CURRENT STATE-OF-ART

Ref.	operation	load type	frequencies	compensation[b]
[3]	dual-band	real	arbitrary	required
[4]	dual-band	complex	arbitrary	not required
[8]	tri-band	real	arbitrary	required
[9]	tri-band	real	restricted	not required
This Work	tri-band	complex[a]	arbitrary	not required

[a]Depends on the type of DBIT.
[b]For different even-odd mode velocities in microstrip.

B. Design Example-II With Type-II DBIT

In this example, $R_L = 20\ \Omega$ is taken to match $Z_0 = 50\ \Omega$. Once again the design procedure provides $Z_{21} = 36.5\ \Omega$, $\theta_{21} = 60°$, $Z_{22} = 109.54\ \Omega$, $\theta_{22} = 60°$, and $Z_{23} = 109.54\ \Omega$, $\theta_{23} = 60°$ for various segments of type-II *DBIT*. Since, instead of 20 Ω resistor, a bit different CRCW series SMD resistor of value 19.6 Ω is available commercially, the designed *DBIT* needed a little optimization. The value of admittance $Y_{\text{in}3}$ @ f_3 is found to be $0.053259 + j0.009097\ \Omega^{-1}$. However, for this value of $Y_{\text{in}3}$, the *DTBT* turns out to be physically unrealizable. Therefore, the *DTBT* was redesigned by incorporating OCSC-2. The impedance Z_c, the free variable, is chosen to be equal to 100 Ω. From the design equations $Z_a = 116.82\ \Omega$, $Z_b = 38.94\ \Omega$, $Z_d = 33.33\ \Omega$, $\theta_1 = 60°$, and $\theta = 13.45°$ are found. The fabricated implemented board is shown in Fig. 2(b) whereas the corresponding EM simulated and measured results given in Fig. 3(b) perfectly demonstrate the tri-band matching capabilities of the proposed design.

The slight anomaly in the measurement and simulation values, of both prototypes, can be overcome by using frequency stable substrate such as RO5880 with $\varepsilon_r = 2.2$.

The comparison of the proposed work with the current state-of-the-art is given in Table I. The novelty of the proposed tri-band matching scheme is apparent as it significantly advances the tri-band matching techniques and will also find definite applications where the earlier techniques couldn't be applied.

V. CONCLUSION

A novel tri-band matching scheme with closed form equations and two design examples have been presented. The measured results show slight deviations and this can be attributed to the choice of substrate RO4350B and the in-house production of boards and this can be addressed by using frequency stable substrate such as RO5880 and professional prototyping. Furthermore, a real and fixed load was assumed in the design examples. However, the presented tri-band matching technique is also extendable to frequency dependent complex load if appropriate complex to real type DBIT is used.

APPENDIX

A. Type-I DBIT

$$G_1 = \frac{R_L(1 + \tan^2 u\theta_{11})}{R_L^2 + Z_{11}^2 \tan^2 u\theta_{11}} \tag{A1a}$$

$$B_1 = \frac{R_L^2 \tan u\theta_{11} - Z_{11}^2 \tan u\theta_{11} + R_L^2 B_L Z_{11} + B_L Z_{11}^3 \tan^2 u\theta_{11}}{Z_{11}(R_L^2 + Z_{11}^2 \tan^2 u\theta_{11})} \tag{A1b}$$

where $B_L = -Y_{12} \cot uq_{12}$ for SC stub and $B_L = -Y_{12} \tan uq_{12}$ for an OC stub with $\theta_{ij}, \forall i, j$ are similar as θ_1.

B. Type-II DBIT

$$G_1 = \frac{R_L(1 + \tan^2 u\theta_{21})}{(1 - B_p Z_{21} \tan u\theta_{21})^2 + (R_L Z_{21} \tan u\theta_{21})^2} \tag{A2a}$$

and (A2b) as shown at the top of the page, where $B_P = -Y_{22} \cot uq_{22}$ for SC stub and $B_P = -Y_{22} \tan uq_{22}$ for an OC stub with $\theta_{ij}, \forall i, j$ are similar as θ_1.

REFERENCES

[1] M. J. Park and B. Lee, "Dual band design of single stub impedance matching networks with application to dual band stubbed T junctions," *Microw. Optic. Tech. Lett.*, vol. 52, no. 6, pp. 1359–1362, Jun. 2010.

[2] Y. Wu, Y. Liu, and S. Li, "A compact Pi-structure dual band transformer," *Prog. in Electromag. Res.*, vol. 88, pp. 121–134, 2008.

[3] M. A. Maktoomi and M. S. Hashmi, "A coupled-line based L-section DC-isolated dual-band real to real impedance transformer and its application to a dual-band T-junction power divider," *Prog. Electromag. Res. C*, vol. 55, pp. 95–104, 2014.

[4] O. Manoochehri, A. Asoodeh, and K. Forooraghi, "Pi-model dual-band impedance transformer for unequal complex impedance loads," *IEEE Microw. Wireless Compon. Lett.*, vol. 25, no. 4, pp. 238–240, Apr. 2015.

[5] M. Chongcheawchamnan, S. Patisang, M. Krairiksh, and I. Robertson, "Tri-band Wilkinson power divider using a three-section transmission line transformer," *IEEE Microw. Wireless Compon. Lett.*, vol. 16, no. 8, pp. 452–454, Aug. 2006.

[6] Z. Wang and W. C. Park, "Concurrent tri-band GaN HEMT power amplifier using resonators in both input and output matching networks," in *Proc. IEEE WAMICON Conf.*, Apr. 2012, pp. 1–4.

[7] Y.-F. Bai, X.-H. Wang, C.-J. Gao, Q.-L. Huang, and X.-W. Shi, "Design of compact quad frequency impedance transformer using two-section coupled line," *IEEE Trans. Microw. Theory Tech.*, vol. 60, no. 8, pp. 2417–2423, Aug. 2012.

[8] X. H. Wang, L. Zhang, Y. Xu, Y. F. Bai, C. Liu, and X.-W. Shi, "A tri-band impedance transformer using stubbed coupling line," *Prog. in Electromag. Res.*, vol. 141, pp. 33–45, 2013.

[9] X. A. Nghiem, J. Guan, T. Hone, and R. Negra, "Design of concurrent multiband Doherty power amplifiers for wireless applications," *IEEE Trans. Microw. Theory Tech.*, vol. 61, no. 12, pp. 4559–4568, Dec. 2013.